CHAPTER VI

PHONON SIDE BANDS IN THE ABSORPTION SPECTRA OF Ni^{2+} AND Co^{2+} IN CdI_2 AND PbI_2

C. Haas, P.R. Boudewijn, S.R. Kuindersma, J. Bethlehem and A. Meetsma

Laboratory of Inorganic Chemistry, Materials Science Center of the University, Nijenborgh 16, 9747 AG Groningen, The Netherlands

ABSTRACT

The absorption and MCD spectra of the $^3A_{2g} \rightarrow {}^1E_g$ electronic transition of $CdI_2:Ni^{2+}$ and $PbI_2:Ni^{2+}$ and of the $a^4T_{1g} \rightarrow b^2T_{1g}$, $^2A_{1g}$ transition of $CdI_2:Co^{2+}$ have been measured. The spectra show a complicated fine structure caused by the coupling with non-localized vibrational modes of the host lattice. The theory of this effect is presented. It is shown that the observed vibronic structure images the phonon density of states in the Brillouin Zone, modified by matrix elements and selection rules. The contributions of the different phonon branches (acoustic, Raman and infrared-active modes) are calculated. The spectra show a strong anisotropy, which is due to the presence of static dipoles at the anions; the magnitude of the anisotropy is calculated using the polarizable-ion model. The vibronic fine structure is used to deduce the maxima of the phonon density of states of CdI_2 and PbI_2, and to estimate the phonon dispersion curves.

CdI_2, PbI_2 and CoI_2 crystallize in the $Cd(OH)_2$ structure, NiI_2 in the $CdCl_2$ structure [1]. The unit cells of both structures can be described hexagonally with the c-axis as the uniaxial axis. Both structures consist of slabs I-M-I; the slabs are interacting only weakly by Van der Waals forces. The metal ion is octahedrally surrounded by six iodine ions. In the diluted systems part of the Cd or Pb ions is replaced by Co^{2+} or Ni^{2+}.

Optical absorption spectra of the first-row transition-metal diiodides inthe visible and near-infrared wavelength region exhibit localized d-d transitions. The pure transition-metal diiodides, especially NiI_2 and CoI_2 also show a strong absorption, due to charge-transfer transitions, which overlap many of the much weaker forbidden d-d transitions. In order to distinguish between single-ion effects and cooperative effects in the spectra, and to examine more d-d transitions, the transition-metal ions were substituted in the diamagnetic host lattices CdI_2 and PbI_2.

The d-d transitions of transition-metal ions substituted on sites with inversion symmetry are parity forbidden for electric-dipole transitions. They become allowed in optical absorption by means of a coupling with vibrations of odd parity. In these cases the zero-phonon transition is observed as a weak magnetic-dipole transition. The electric-dipole transitions occur as vibronic side bands.

In the literature there are numerous examples of complicated vibronic fine structures, simple phonon progressions and combinations of both phenomena. The type of vibronic side band that is observed, depends strongly on the magnitude of the lattice distortion and of the vibronic coupling. Bron and Wagner [2] distinguished four combinations of the magnitude of the lattice distortions due to the ion substitution and the electron-phonon coupling. A small lattice distortion and a weak coupling lead to one-phonon processes, as observed for instance for intraconfigurational transitions $4f^n \rightarrow 4f^n$ of Pr^{3+} in $LaCl_3$ [3]. The observed maxima in this spectrum are ascribed to singular points in the Brillouin Zone of $LaCl_3$, and the spectrum reflects the phonon density of states of $LaCl_3$, modified by vibronic selection rules. In the case of a large lattice distortion and a strong coupling the spectrum consists of a long series of sharp phonons associated with an electronic transition involving a configurational change, for instance $4f^n \rightarrow 4f^{n-1}5d$. The coupling of the localized mode with the lattice modes of the host crystal is weak, and

the observed phonons are ascribed to the localized mode. The case of a small lattice distortion and a strong coupling leads to progressions of non-localized phonons over a broad frequency region. For a large distortion and a weak coupling the phonons are strongly altered by the distortion. In this case localized modes may be visible in the spectra. Again, due to the weak coupling, a limited structure of mainly one-phonon lines is expected.

For crystals with defects (substituted ions) the influence of the defect atom on the vibrational modes should be taken into account. Not only mass defects should be considered but also changes in the force constants.

Barker and Sievers [4] discussed the vibrational properties of crystals, in which particular mass substitutions were made. Explicit calculations were carried out for a linear chain of atoms. The dispersion curves of the pure diatomic chain in the first Brillouin Zone consist of acoustic and optic bands, separated by a gap at the edge of the Brillouin Zone. The low-frequency acoustic band corresponds mainly to the vibrations of heavy atoms, whereas in the high-frequency optic band the light element has the largest amplitude. If the nearest-neighbour force constants are unchanged a localized mode is created, if the light element is replaced. Depending on the weight of the substituted defect the frequency of the localized mode is larger or smaller than the maximum or minimum frequency of the optic band. These two types of localized modes are called the local and gap mode, respectively. In addition to the creation of the localized mode the band-mode amplitudes are modified in the neighbourhood of the defect, giving rise to a weak infrared absorption. If a heavy atom in the chain is replaced by a lighter one, two localized modes are obtained, a local mode and a gap mode. Substitution of a heavier isotope for the heavy atom in the chain does not result in localized modes, but only in a slight modification of the band modes. A reduction of the force constant which links the defect with its neighbours, can lead to resonant modes, in which the defect has a large amplitude. It is expected that this type of modes plays an important role in compounds that do not exhibit a large gap between the acoustic and optic bands, such as CdI_2 and PbI_2.

The crystal-field transitions of the system $CaO:Ni^{2+}$ have been investigated in great detail [5,6]. Because Ca^{2+} has been replaced by the heavier Ni^{2+} ion and the force constants with nearest-neighbour ions are likely to be reduced, a resonant mode is expected. Electric-dipole transitions from the ground state $^3A_{2g}(e_g^2)$ to the excited states $^1T_{2g}(t_{2g}e_g)$, $^3T_{1g}(t_{2g}e_g)$ show a number of peaks at the low-frequency sides of broad bands. These peaks are

ascribed to a vibronic coupling of the electronic states with a resonant mode of t_{1u} symmetry.

Sangster and McCombie [7] have considered the emission spectrum of the $^2E_g(t_{2g}^3) \rightarrow {}^4A_{2g}(t_{2g}^3)$ transition of V^{2+} in MgO. A comparison of the phonon side bands of electronic transitions in $MgO:Ni^{2+}$ and $MgO:V^{2+}$ shows that the bands are very sensitive to modifications of the modes in the immediate vicinity of the defect ion. Three localized t_{1u} modes were taken into account; one t_{1u} modulates the transition metal-ligand distance, the second changes the ligand-metal-ligand angle and the third is a translational mode. The response of the lattice to the change of the mass and the force constants has been evaluated with a Green's function method. Only displacements of the impurity ion and its nearest neighbours were coupled to the electronic transition. The largest contribution appeared to arise from the localized t_{1u} which modulates the metal-ligand distance.

In this article we discuss the absorption and magnetic circular dichroism (MCD) spectra of the isoconfigurational transition $^3A_{2g}(e_g^2) \rightarrow {}^1E_g(e_g^2)$ in $CdI_2:Ni^{2+}$ [8] and $PbI_2:Ni^{2+}$ and related transitions in $CdI_2:Co^{2+}$ [9,10]. The spectra show a zero-phonon magnetic-dipole transition and fine structures due to vibronic side bands. The fine structure can be related to the phonon density of states of the host lattice. The general theory of the coupling of parity-forbidden electronic transitions located at the defect ion, with the vibrational modes of the host lattice is given. The theory is applied to layered diiodides; the anisotropy of the coupling is attributed to the vibrational anisotropy of the layered compounds. The contributions of the various phonon branches in the Brillouin Zone to the fine structure in the spectra are calculated. Finally, the maxima in the fine structures are assigned to the maxima in the phonon density of states, which correspond to flat regions of the dispersion curves near symmetrical points in the Brillouin Zone. Tentative dispersion curves of CdI_2 are estimated from the assignments of the spectra.

VI.2 EXPERIMENTAL PART

CdI_2, PbI_2, NiI_2 and CoI_2 were prepared from the elements in evacuated quartz ampoules at temperatures of 350, 470, 700 and 500°C, respectively. Also commercial CdI_2 was used after sublimation at about 450°C. The solid solutions were synthesized with the Bridgman technique. A powder of CdI_2 or PbI_2 was mixed with a small amount of NiI_2 or CoI_2, and put in a small quartz tube.

The evacuated tubes were kept for several days at a temperature of 450°C in the case of CdI_2 or at 500°C in the case of PbI_2, and then carefully lowered through the temperature gradient. From the ingots it is easy to cut single crystal plates perpendicular to the c-axis; these plates are used for recording the axial spectra. In order to obtain crystal plates with the c-axis parallel to the crystal plane, the samples were embedded in a two-component thermosetting resin (Buehler). The crystals were carefully sawn with a diamond saw. Some of the crystals were polished with powders, other crystals were cleaned with an ethanol-wet wash leather. The optical quality of these crystals is less than that of the naturally cut crystals, used for the axial spectra.

The 3d-metal ion concentration was determined by chemical analysis. In the $CdI_2:Co^{2+}$ samples the Co^{2+} concentration varied from 0.5 to 0.88 mol %. The $CdI_2:Ni^{2+}$ crystal contained 0.1 mol % of NiI_2. The chemical analysis of $PbI_2:Ni^2$ revealed a concentration as large as 2.0 mol % NiI_2. A microscopic study, however, showed the presence of some dark rings, probably due to an enhanced local concentration of Ni.

The transmission and MCD spectra were recorded with a Perkin-Elmer E-1 monochromator. The sample was mounted in an Oxford Instruments SM 4 cryostat, providing magnetic fields up to 5 T. The temperature was varied from 1.5 to 300 K. The resolution was about 2 cm^{-1}.

In *Figure VI.1* the absorption (α,π-polarized) and MCD spectra at 4.2 K of the $^3A_{2g} \rightarrow {}^1E_g$ transition of $CdI_2:Ni^{2+}$ are shown. The absorption spectra were recorded for the configurations α ($E \perp c$, $H \perp c$), π ($E//c$, $H \perp c$) and σ ($E \perp c$, $H//c$). The MCD spectrum was recorded with the light propagating along the c-axis and the magnetic field parallel to the c-axis. The absorption spectrum changes only slightly between 4.2 K and 30 K; above 30 K a broadening is observed. The observed sharp features with splittings of a few wave numbers do not correspond to the known frequencies at $k = 0$ of CdI_2. Striking is the different shape of the bands labelled 1 and 2. Whereas band 1 is symmetric, band 2 has a long tail to lower energies. Another remarkable feature is the sharp cut-off of the spectra at about 12600 cm^{-1}.

There is a reduction of the intensities in the π-polarized spectrum as compared with those of the α-polarization. The positions of the peaks in both spectra coincide. An exception is the behaviour of band number 7, the intensity of which does not reduce from α to π.

The MCD spectrum consists of temperature-dependent C-terms [11]. Band 1 at 12441 cm^{-1} has an opposite sign to that of the rest of the spectrum, and

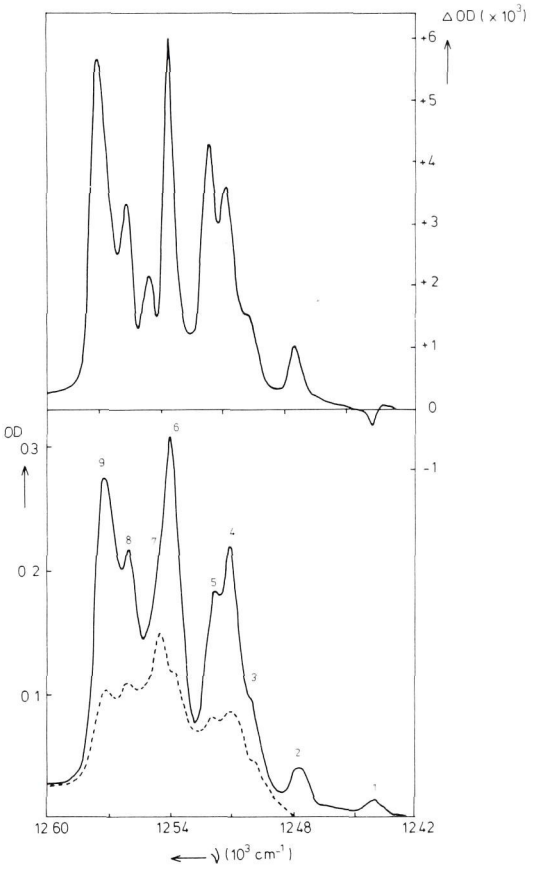

Figure VI.1: Absorption (lower part) and MCD spectra (upper part) of the $^3A_{2g} \rightarrow {}^1E_g$ *transition in* $CdI_2:Ni^{2+}$ *at 4.2 K. The figure gives the OD (optical density) and ΔOD as a function of photon energy. The magnetic field of the MCD is 10 kG. The solid curve is the α- and the broken curve is the π-polarized absorption.*

is assigned to the zero-phonon magnetic-dipole transition. A comparison of the line width of bands 6, 7 in absorption and MCD indicates that the MCD consists of two contributions of opposite sign.

In *Figure VI.2* the absorption (α-polarized) and MCD spectra at 2.1 K of $PbI_2:Ni^{2+}$ are shown. The frequency region is the same as for $CdI_2:Ni^{2+}$, and the fine structure is assigned to the $^3A_{2g} \rightarrow {}^1E_g$ transition. Although a chemical analysis of $PbI_2:Ni^{2+}$ crystals revealed a Ni^{2+} concentration of 2 mol % we believe that the local concentration is much lower. The absorption and MCD signals are much weaker than those of $CdI_2:Ni^{2+}$ (0.1 mol %).

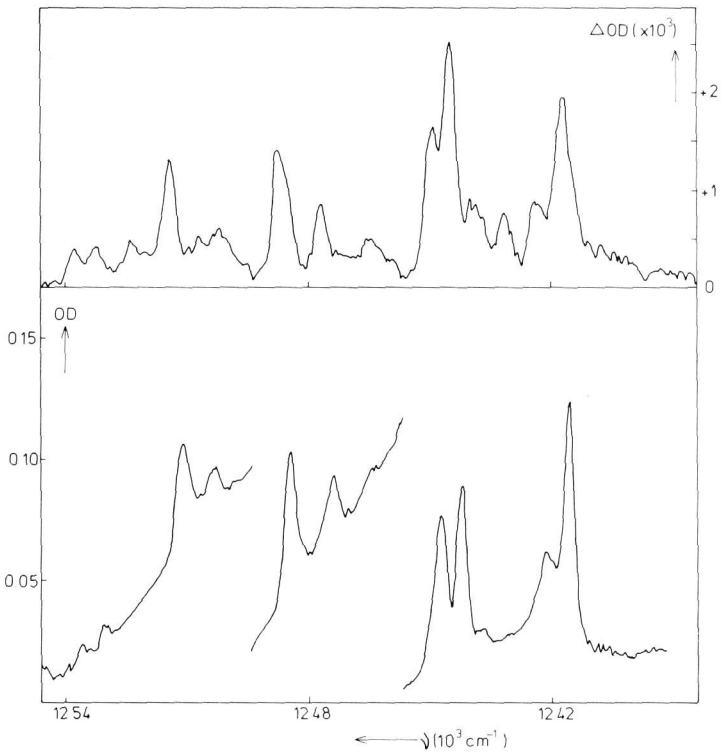

Figure VI.2: Absorption (lower part) and MCD spectra (upper part) of the $^3A_{2g} \rightarrow {}^1E_g$ *transition in* $PbI_2:Ni^{2+}$ *at 2.1 K. The figure gives the OD and ΔOD versus photon energy. The absorption is α-polarized. The magnetic field of the MCD is 40 kG.*

The spectra of $PbI_2:Ni^{2+}$ again show sharp vibronic features. The width of the spectrum is about 120 cm^{-1}. Apart from the sharp peaks in the absorption spectrum, there is a broad background. This background is not observed in the MCD spectrum; the background was absent in crystals with a much lower Ni^{2+} concentration.

σ- and π-polarized absorption spectra of $PbI_2:Ni^{2+}$ showed the same absorption peaks as the α-polarized spectrum. However, the signal-noise ratio and resolution was bad. The maxima in the MCD spectrum correspond to the maxima in the α-polarized absorption spectrum. The band at 12394 cm^{-1} (*Figure VI.2*) has a MCD sign opposite to that of the rest of the spectrum, and is assigned to the zero-phonon transition.

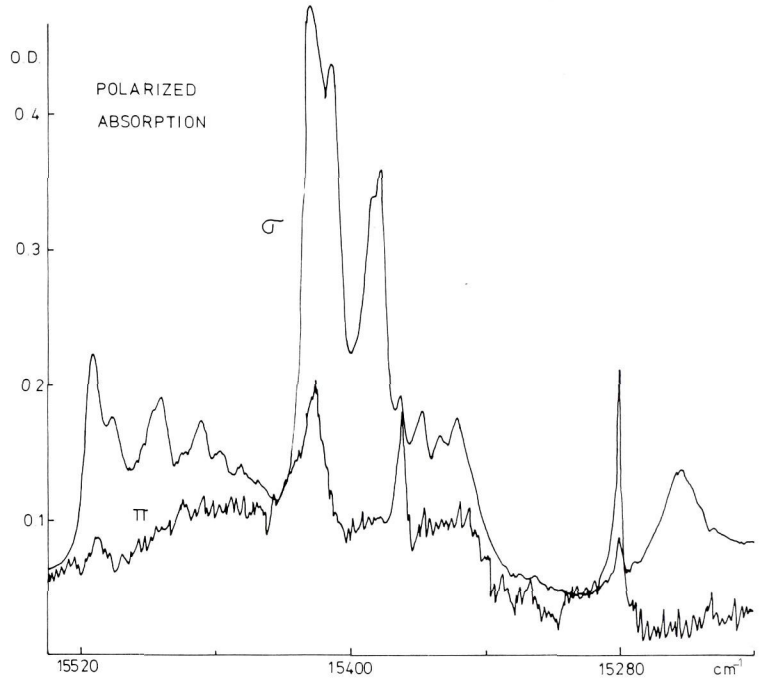

Figure VI.3: Polarized absorption spectra of the $a^4T_{1g} \rightarrow b^2T_{1g}$ *transition in* $CdI_2:Co^{2+}$ *at 4.2 K.*

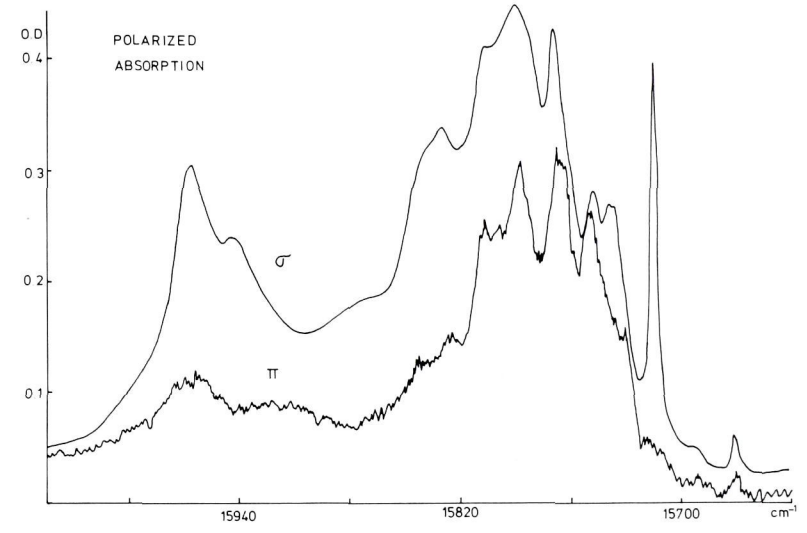

Figure V.4: Polarized absorption spectra of the $a^4T_{1g} \rightarrow {}^2A_{1g}$ *transition in* $CdI_2:Co^{2+}$ *at 4.2 K.*

Figures VI.3 and *VI.4* show the σ- and π-polarized spectra of spin-forbidden transitions in CdI_2:Co^{2+} (0.88 mol %). A detailed assignment of the CdI_2:Co^{2+} spectra will be reported later [10]. *Figure VI.3* shows the $a^4T_{1g}(t_{2g}e_g^2) \rightarrow b^2T_{1g}(t_{2g}e_g^2)$ transition of the Co^{2+} ion (d^7). The excited state is split by spin-orbit coupling into two components U'_g and E'_g; the zero-phonon transitions are observed at 15280 cm^{-1} and 15376 cm^{-1}, respectively. The irregular pattern is originating from the phonon density of states of CdI_2. The spectrum of the E'_g is a repetition of the spectrum of the U'_g, although it is much weaker. *Figure VI.3* shows the strong reduction in intensity from σ to π polarization.

Figure VI.4 shows the vibronic fine structure of the $a^4T_{1g}(t_{2g}e_g^2) \rightarrow {}^2A_{1g}(t_{2g}^2e_g)$ transition. The band at 15669 cm^{-1} is assigned to the magnetic-dipole transition. The maxima in the vibronic side band of the σ spectrum are broadened with respect to those in the spectrum of *Figure VI.3*. The sharp cut-off at the high-frequency side (*Figures VI.1* and *VI.3*), characteristic for one-phonon processes, is not observed for the ${}^2A_{1g}$ transition. This is presumably due to two-phonon processes. An additional peak is observed at 15716 cm^{-1}. Whereas the fine structure shows a reduction from σ to π polarization, the peak at 15716 cm^{-1} is completely σ polarized.

Lists of observed positions of the maxima in the doped CdI_2 and PbI_2 systems are given in Section VI.4, together with the assignments to special points in the Brillouin Zones.

VI.3 THEORETICAL PART

VI.3.1 General theory of vibronic coupling

In this section we discuss the complex problem of the coupling of the many-electron states of a transition metal with the vibrations of the crystal in which the ion is incorporated as an impurity. The total Hamiltonian for this problem is

$$H = \sum_i h_o(i) + \sum_{ij} h_{ij} + H_{so} + T_N + V_N \qquad (1)$$

The first term is a sum over one-electron Hamiltonians for electrons i, the second term represents the electron-electron interaction, H_{so} is the spin-orbit interaction and T_N and V_N are the kinetic energy and interaction energy of the nuclei in the system. The total wave function of the system can be constructured in the following way. First the one-electron Hamiltonian of elec-

tron i is considered:

$$h_o(r_i, R_M, R_L) = -\frac{\hbar^2}{2m}\nabla_i^2 + V(r_i, R_M, R_L) \tag{2}$$

It consists of a kinetic energy, and a potential energy V, representing the interaction of electron i (coordinate r_i) with the nuclei (transition metal at position $\underline{R}_M$, ligand atoms at positions $\underline{R}_L$), and with all other electrons. The solutions of equation (2) are one-electron molecular orbitals Φ_m, which can be expressed as a linear combination of atomic orbitals.

$$\Phi_m = N_m\left\{\phi_d^m(r_i - R_M) + \sum_j \rho_{mj}\phi^j(r_i - R_M) + \sum_L \sum_t \lambda_{mLt}\phi_L^t(r_i - R_L)\right\} \tag{3}$$

ϕ_d^m (m = 1-5) are the transition-metal d orbitals, ϕ^j are any other atomic orbitals of the transition-metal atom, and ϕ_L^t are atomic orbitals of the ligand atoms. N_m is a normalization constant.

We will consider transitions involving electrons which have predominantly d character; in that case the coefficients ρ_{mj} and λ_{mLt} (which represents the covalent mixing of metal d with ligand orbitals) are small.

The electronic wave function is obtained from the electronic Hamiltonian

$$H_e = \sum_i h_o(i) + \sum_{ij} h_{ij} + H_{so} \tag{4}$$

$$H_e\psi_e(r_1 \ldots r_i, R_M, R_L) = \varepsilon_e(R_M, R_L)\psi_e(r_1 \ldots r_i, R_M, R_L) \tag{5}$$

This many-electron wave function, which still depends on the nuclear coordinates, can be written as a linear combination of Slater determinants, constructed from one-electron molecular orbitals derived above. The spin-orbit interaction H_{so} for 3d electrons is small and will be treated as a pertubation.

In the spirit of the Born-Oppenheimer approximation [12] the total wave function is written as

$$\Psi = \psi_e(r_1 \ldots r_i, R_M, R_L)\,\chi(R_M, R_L) \tag{6}$$

The electron energy $\varepsilon_e(R_M,R_L)$ serves as a potential energy for the nuclear vibrations; the vibrational wave functions χ are obtained from

$$\left\{T_N + \varepsilon_e(R_M,R_L)\right\} \chi = E\chi \tag{7}$$

We consider only vibrations of small amplitude around the equilibrium nuclear configurations R_M^o,R_L^o, which we assume to be the same for all electronic states to be considered. The latter is a reasonable assumption for the discussion of transitions between isoconfigurational electronic states. In this approximation the vibrations are independent of the electronic state, and are in the harmonic approximation characterized by normal coordinates for independent harmonic vibrations. For an unperturbed crystal the normal coordinates Q_{ki} are delocalized, and are characterized by a wave vector $\underline{k}$ (i denotes the vibrational branch number). For a crystal containing an impurity ion generally one distinguishes delocalized modes Q_{ki}, derived from the normal modes of the unperturbed crystal, and local (gap) modes Q_l [4]. The normal coordinates Q_{ki} are similar to those of the unperturbed crystal, except for the immediate vicinity of the impurity atom. The total energy is given by

$$E = \varepsilon_e + \sum_{k,i} (n_{ki} + \tfrac{1}{2})\,\hbar\omega_{ki} + \sum_{l} (n_l + \tfrac{1}{2})\,\hbar\omega_l \tag{8}$$

where ω_{ki} and ω_l are the angular frequencies of modes Q_{ki} and Q_l, respectively.

We now consider an optical electric-dipole transition between two electronic states a and b; the transition moment for light polarized with the electric vector in the β direction, is given by

$$m_{ab}^{\beta} = \langle \psi_a\, \chi_a | \sum_i m_\beta(r_i) | \psi_b\, \chi_b \rangle \tag{9}$$

where $m_\beta(r_i)$ are the components of the electronic dipole operator $\underline{m} = e\underline{r}_i$. The electronic transition moments for a fixed non-equilibrium configuration of the nuclei (R_M,R_L) is

$$P_{ab}^{\beta}(R_M,R_L) = \langle \psi_a(r_i,R_M,R_L) \mid \sum_i m_\beta(r_i) | \psi_b(r_i,R_M,R_L) \rangle \tag{10}$$

For a d-d transition of a transiton-metal ion at a site with inversion symmetry, P^{β}_{ab} vanishes for the equilibrium nuclear configuration. Therefore, in order to obtain a non-vanishing transition probability, it is necessary to consider first-order terms linear in the nuclear displacements. For this purpose the electronic Hamiltonian H_e is written as

$$H_e(r_1 \ldots r_i, R_M, R_L) = H^o_e(r_1 \ldots r_i, R^o_M, R^o_L) + H_v \tag{11}$$

The vibronic interaction H_v is treated as a pertubation.

For a transition-metal atom in an octahedral coordination it is expected that the vibronic coupling will be predominantly with t_{1u} local displacements of the octahedron of ligand atoms, which modulate the metal-ligand distance [7,13,14]. If only the interaction with this type of displacements is considered, we obtain in first approximation

$$H_v = \sum_{\rho} \Delta U^{t_{1u}}_{\rho}(r_1 \ldots r_i) q^{t_{1u}}_{-\rho} \tag{12}$$

where $q_{-\rho}$ is the amplitude of the t_{1u}-type displacements with components $\rho = 0, \pm 1$.

With these assumptions it is possible to evaluate the electronic-transition matrix elements P^{β}_{ab} with pertubation theory, treating H_{so} and H_v as small pertubations. These matrix elements are quite complicated for the many-electron wave functions involved, and can be evaluated using the irreducible tensor method (Section VI.3.2) [15].

The electronic-transition matrix element depends linearly on the local amplitudes $q_{-\rho}$

$$P^{\beta}_{ab} = \sum_{\rho} B^{\beta\rho}_{ab} q_{-\rho} \tag{13}$$

The local distortions can be decomposed into the normal vibrations of the crystal:

$$q_{\rho} = \sum_{k} \sum_{i} S^{\rho}_{ki} Q_{ki} + \sum_{l} S^{\rho}_{l} Q_l \tag{14}$$

The absorption coefficient $\alpha(\omega)$ for a transition $a \rightarrow b$ at low temperature, when all phonon modes (k,i) are in the vibrational ground state $n_{ki} = 0$,

$n_l = 0$, is given by

$$\alpha_\beta(\omega) = c \sum_{a\to b} \left\{ \sum_k \sum_i |\langle n_{ki} = 0|P^\beta_{ab}|n_{ki} = 1\rangle|^2 \, \delta(\omega = \omega_o + \omega_{ki}) + \right.$$
$$\left. + \sum_l |\langle n_l = 0|P^\beta_{ab}|n_l = 1\rangle|^2 \, \delta(\omega = \omega_o + \omega_l) \right\} \qquad (15)$$

where c is a constant, β gives the polarization direction of the light, and the summation is over all components of ground state a and excited electronic state b. The frequency ω_o corresponds to the zero-phonon energy separation of initial and final state. Using $\langle n = 0|Q|n = 1\rangle = (\hbar/2\omega)^{\frac{1}{2}}$ for a harmonic oscillator of frequency ω, one obtains

$$\alpha_\beta(\omega) = c \sum_{a\to b} \sum_{\rho\rho'} (B^{\beta\rho}_{ab})^*(B^{\beta\rho'}_{ab}) \times$$
$$\times \left\{ \sum_{ki} (\hbar/2\omega_{ki})(S^\rho_{ki})^*(S^{\rho'}_{ki}) \, \delta(\omega = \omega_o + \omega_{ki}) + \right.$$
$$\left. + \sum_l (\hbar/2\omega_l)(S^\rho_l)^*(S^{\rho'}_l) \, \delta(\omega = \omega_o + \omega_l) \right\} \qquad (16)$$

From this expression the shape of the absorption spectrum can be calculated, if the coefficients S^ρ_{ki} and S^ρ_l are known.

VI.3.2 Theory of the $^3A_{2g} \to {}^1E_g$ electronic transition of Ni^{2+} in an octahedral coordination

In this section we consider the electronic transition $^3A_{2g} \to {}^1E_g$ of a Ni^{2+} ion in an octahedral coordination of ligand ions. Both the ground state $^3A_{2g}$ and the excited state ^1E_g are derived from the same strong-field configuration e_g^2. Thus the $^3A_{2g} \to {}^1E_g$ transition is isoconfigurational. One expects only a weak electron-phonon coupling, and no appreciable Franck-Condon effect.

The $^3A_{2g} \to {}^1E_g$ transition is allowed as a magnetic-dipole transition through spin-orbit coupling of the excited state with the $^3T_{2g}$ state. For low magnetic field ($g\mu_B H \ll kT$) the magnetic circular dichroism (MCD) is proportional to [11]

$$\sum_{a\to b} \langle a|\mu_z|a\rangle \left\{ |\langle a|\mu_+|b\rangle|^2 - |\langle a|\mu_-|b\rangle|^2 \right\} \qquad (17)$$

where μ_z, $\mu_\pm$ are the magnetic moment operators. The summation is over all components of ground and excited state. For the $^3A_{2g} \rightarrow {}^1E_g$ magnetic-dipole transition a negative MCD signal is calculated.

In the case of spin- and parity-forbidden electric-dipole transitions the spin-orbit coupling and the vibronic coupling together provide a number of mechanisms through which the transition may become allowed. Using pertubation theory, the relative importance of different processes can be estimated by comparing the energy denominators, which appear in the expressions for the transition probability. Due to the relative closeness of the ^1E_g and the $^3T_{1g}$ and $^3T_{2g}$ states we have limited our calculations to the two processes depicted in *Figure VI.5*. Assuming that the dominant part comes from t_{1u} vibrations, as

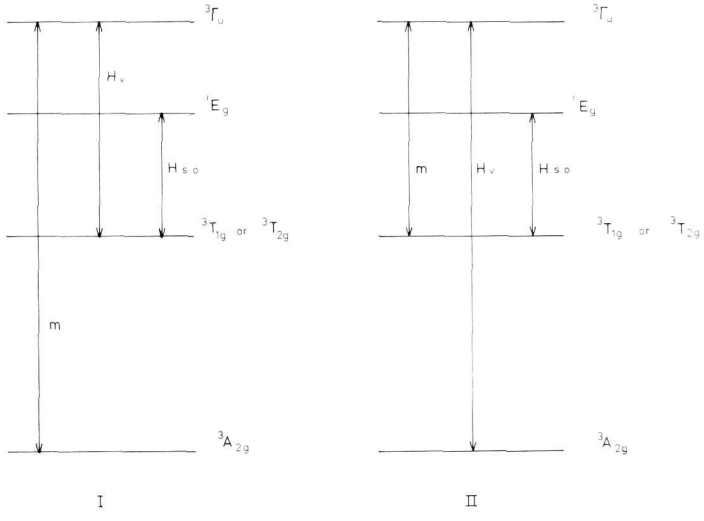

Figure VI.5: Vibronic and spin-orbit coupling mechanisms, which make the $^3A_{2g} \rightarrow {}^1E_g$ transition in CdI_2:Ni^{2+} electric-dipole allowed.

is observed in other Ni^{2+} systems [13,14], the intermediate states $^3\Gamma_u$ will be $^3T_{2u}$. The transition moment for coupling with $^3T_{2g}$ is given by equation (18).

The states are labelled by their O_h^* double-group representation, with in brackets the O_h representation. Vibrational states are indicated by $\nu(a_{1g})$ and $\nu(t_{1u})$ for ground and excited state, respectively (low-temperature approximation with only the lowest vibrational level of the ground state populated). Using V coefficients the coupled functions $T_{2g}(^3A_{2g})\gamma$ and $E_g(^3T_{2g})\gamma'$ can be expressed in the uncoupled functions [15]. Integration over the spin coordi-

$$\langle T_{2g}(^3A_{2g})\gamma\cdot\nu(a_{1g})\iota|m_\beta|E_g(^1E_g)\gamma'\cdot\nu(t_{1u})\tau\rangle =$$

$$= \sum_{\kappa}\sum_{M_s}\sum_{\rho}\left\{\langle T_{2g}(^3A_{2g})\gamma|m_\beta|\ ^3T_{2u}M_s\kappa\rangle\langle ^3T_{2u}M_s\kappa|\Delta U^{t_{1u}}|E_g(^3T_{2g})\gamma'\rangle \times\right.$$

$$\times\frac{1}{[E(^3T_{2g}) - E(^3T_{2u})]} + \langle T_{2g}(^3A_{2g})\gamma|\Delta U^{t_{1u}}|^3T_{2u}M_s\kappa\rangle\langle ^3T_{2u}M_s\kappa|m_\beta|E_g(^3T_{2g})\gamma'\rangle \times$$

$$\left.\times\frac{1}{[E(^3A_{2g}) - E(^3T_{2u})]}\right\}\frac{\langle E_g(^3T_{2g})\gamma'|H_{so}|E_g(^1E_g)\gamma'\rangle\langle a_{1g}\iota|q_{-\rho}^{t_{1u}}|t_{1u}\tau\rangle}{[E(^1E_g) - E(^3T_{2g})]} \qquad (18)$$

nates and using the Wigner-Eckart theorem make it possible to express the result in terms of V coefficients and reduced matrix elements. The V coefficients for the complex trigonal component system are given in Appendix A. The result is

$$\langle T_{2g}(^3A_{2g})\gamma\cdot\nu(a_{1g})\iota|m_\beta|E_g(^1E_g)\gamma'\cdot\nu(t_{1u})\tau\rangle =$$

$$= \sum_{M_s}\sum_{j} -(1/\sqrt{6})\, V\begin{pmatrix} A_{2g} & T_{1g} & T_{2g} \\ \iota & M_s & -\gamma \end{pmatrix} V\begin{pmatrix} T_{2g} & T_{1g} & E_g \\ j & M_s & -\gamma' \end{pmatrix}\varepsilon_{\beta j\tau} M_2 \qquad (19)$$

where we have used the fact that the matrix element of the spin-orbit coupling operator is $(1/2)\sqrt{6}\zeta'$ and

$$M_2 = \zeta'\left\{\langle ^3A_{2g}||m||^3T_{2u}\rangle\langle ^3T_{2u}||\Delta U^{t_{1u}}||^3T_{2g}\rangle/\Delta E_1 + \right.$$

$$\left. + \langle ^3A_{2g}||\Delta U^{t_{1u}}||^3T_{2u}\rangle\langle ^3T_{2u}||m||^3T_{2g}\rangle/\Delta E_2\right\}\langle a_{1g}||q^{t_{1u}}||t_{1u}\rangle/\Delta E_3 \qquad (20)$$

with

$$\begin{aligned}\Delta E_1 &= E(^3T_{2g}) - E(^3T_{2u}) \\ \Delta E_2 &= E(^3A_{2g}) - E(^3T_{2u}) \\ \Delta E_3 &= E(^1E_g) - E(^3T_{2g})\end{aligned} \qquad (21)$$

The expressions obtained for coupling with the $^3T_{1g}$ are

$$\langle T_{2g}(^3A_{2g})\gamma\cdot\nu(a_{1g})\iota|m_\beta|E_g(^1E_g)\gamma'\cdot\nu(t_{1u})\tau\rangle =$$

$$= \sum_{M_s}\sum_{j} -V\begin{pmatrix} A_{2g} & T_{1g} & T_{2g} \\ \iota & M_s & -\gamma \end{pmatrix} V\begin{pmatrix} T_{1g} & T_{1g} & E_g \\ j & M_s & -\gamma' \end{pmatrix} V\begin{pmatrix} T_{1g} & T_{1u} & T_{2u} \\ j & \beta & \tau \end{pmatrix} M_1 \qquad (22)$$

with $M_1 = \zeta'\left\{\langle {}^3A_{2g}||m||{}^3T_{2u}\rangle \langle {}^3T_{2u}||\Delta U^{t_{1u}}||{}^3T_{1g}\rangle/\Delta E_1' + \right.$

$$\left. + \langle {}^3A_{2g}||\Delta U^{t_{1u}}||{}^3T_{2u}\rangle \langle {}^3T_{2u}||m||{}^3T_{1g}\rangle/\Delta E_2\right\} \langle a_{1g}||q^{t_{1u}}||t_{1u}\rangle/\Delta E_3' \qquad (23)$$

and

$$\Delta E_1' = E(^3T_{1g}) - E(^3T_{2u})$$
$$\Delta E_3' = E(^1E_g) - E(^3T_{1g}) \qquad (24)$$

TABLE VI.1: Transition intensities for the $^3A_{2g} \rightarrow {}^1E_g(t_{1u})$ transition. The numbers in brackets give the component of the t_{1u} vibration involved in the transition.

		Coupling with $^3T_{1g}$ (in units of $A = M_1^2/324$)		Coupling with $^3T_{2g}$ (in units of $B = M_2^2/108$)	
		^1E_g +1	^1E_g -1	^1E_g +1	^1E_g -1
m_+					
$^3A_{2g}$	-1	A (0)	A (+1)	B (0)	B (-1)
	0	4A (-1)	A (0)	0	B (0)
	+1	A (+1)	4A (-1)	B (-1)	0
m_-					
$^3A_{2g}$	-1	4A (+1)	A (-1)	0	B (+1)
	0	A (0)	4A (+1)	B (0)	0
	+1	A (-1)	A (0)	B (+1)	B (0)
m_o					
$^3A_{2g}$	-1	A (-1)	4A (0)	B (+1)	0
	0	A (+1)	A (-1)	B (-1)	B (+1)
	+1	4A (0)	A (+1)	0	B (-1)

The calculated transition intensities for the components of the $^3A_{2g} \rightarrow {}^1E_g(t_{1u})$ transition for different polarizations are given in Table VI.1. Knowing that the lowest Zeeman level is the $^3A_{2g}$-1 component, the sign of the MCD is easily calculated; it is found that coupling with $^3T_{1g}$ results in a positive MCD signal, coupling with $^3T_{2g}$ in a negative MCD signal. The observed positive MCD signal for vibronic side bands indicates that spin-orbit coupling with $^3T_{1g}$ dominates, which is not surprising in view of the small energy difference between ^1E_g and the $^3T_{1g}$ state [16] (Chapter V).

VI.3.3 Vibronic coupling in $Cd(OH)_2$-type layered compounds

In this part we discuss the lattice vibrations of crystals with the $Cd(OH)_2$-type structure, and the vibronic coupling of these vibrations with electronic transitions at an impurity ion.

The unit cell of the $Cd(OH)_2$-type structure contains two anions and one metal ion. A factor-group analysis yields nine normal modes Q_i at k = 0 (*Figure VI.6*). Three modes are acoustic modes, transforming in D_{3d} symmetry as E_u and A_{2u}. The three infrared-active modes also transform as E_u and A_{2u}. The Raman modes are characterized as E_g and A_{1g}. The E modes have atomic displacements parallel to x and y, the A modes displacements parallel to z.

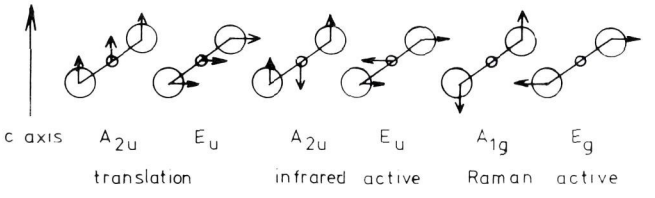

Figure VI.6: The nine normal modes at k = 0 of the $Cd(OH)_2$ structure.

For a proper analysis of the vibronic coupling the normal vibrations of the crystal as modified by the impurity ion should be used. This requires solving the full dynamical matrix of host lattice plus impurity ion. An analysis of this type has not been given so far, and explicit expressions of the normal modes are not available. In this section we will employ a highly simplified model of vibrational modes. In the first place we neglect the specific influence of the impurity ion, *i.e.* we assume the same vibrations as for the pure host crystal. This corresponds not only to neglecting local modes and gap

modes, but also to neglecting local modifications of the normal coordinates in the vicinity of the impurity ion. Secondly, we assume that the nine phonon branches do not mix. This is a very crude approximation, which is certainly not valid at points in the Brillouin Zone where branches are close to one another. Finally, we consider only vibrations within one MI_2 slab, *i.e.* we neglect dispersion of lattice vibrations in the direction parallel to the c-axis.

The local amplitudes of the metal u_M and of the iodines u_L and $u_{L'}$ are

$$u_M^{n\alpha} = (M)^{-\frac{1}{2}} \sum_k \sum_i C_{Mi}^{\alpha} Q_{ki} e^{-ikn} \tag{25}$$

$$u_L^{n\alpha} = (m)^{-\frac{1}{2}} \sum_k \sum_i C_{Li}^{\alpha} Q_{ki} e^{-ikn} \tag{26}$$

$$u_{L'}^{n\alpha} = (m)^{-\frac{1}{2}} \sum_k \sum_i C_{L'i}^{\alpha} Q_{ki} e^{-ikn} \tag{27}$$

where $n = n_1\underline{a}_1 + n_2\underline{a}_2$ denotes the two-dimensional unit cell, α describes the cartesian x, y and z axes, M is the mass of the metal ion and m is the mass of the anion. The assumptions correspond to using k-independent coefficients C; the k dependence of the displacements is restricted to the phase factor e^{-ikn}.

The coefficients C are readily calculated from the k = 0 modes. For the acoustic modes (i = 1-3) we obtain

$$C_{Mi}^{\alpha} = C_{Li}^{\alpha} = C_{L'i}^{\alpha} = N^{-\frac{1}{2}} (M + 2m)^{-\frac{1}{2}} \tag{28}$$

For the infrared modes (i = 4-6) the coefficients are

$$C_{Mi}^{\alpha} = N^{-\frac{1}{2}} M^{-1} \left\{1/M + 1/(2m)\right\}^{-\frac{1}{2}}$$

$$C_{Li}^{\alpha} = C_{L'i}^{\alpha} = -N^{-\frac{1}{2}} (2m)^{-1} \left\{1/M + 1/(2m)\right\}^{-\frac{1}{2}} \tag{29}$$

The Raman modes (i = 7-9) have coefficients

$$C^{\alpha}_{Mi} = 0$$

$$C^{\alpha}_{Li} = -C_{L'i} = N^{-\frac{1}{2}} (2m)^{-\frac{1}{2}} \qquad (30)$$

In these formula N is the number of unit cells per unit volume.

In the previous section we emphasized that the modulation of the metal-ligand distance is mainly responsible for the coupling of the vibrations with the electronic transition. The next step is to write the three components of the local distortion t_{1u} of the NiI_6^{4-} octahedron in terms of atomic displacements of Ni^{2+} and the six ligand iodine ions. Then, using equations (25)-(30), it is possible to derive expressions for the local t_{1u} distortion of the NiI_6^{4-} octahedron in terms of the normal coordinates of the crystal. In this way the coefficients S^{ρ}_{ki} of equation (14) are calculated.

The site symmetry of the Ni^{2+} ion in CdI_2 and PbI_2 is not octahedral, but rather D_{3d}. As the trigonal field is small its influence on the electronic states can be neglected, and the electronic states can be labelled according to their O_h representation. On the other hand, it is well known that the influence of the trigonal field, especially the influence of the static dipoles at the iodine ions, on the vibrational frequencies and oscillator strengths is appreciable (Chapter IV) [17,18]. Therefore, a localized t_{1u} distortion should be decomposed into a_{2u}- and e_u-type distortions (site symmetry D_{3d}). The $\rho = 0$ component of t_{1u} corresponds to a_{2u} and the $\rho = \pm 1$ components to e_u. It is expected that this anisotropy will lead to different vibronic coupling strengths for $t_{1u}(0)$ and $t_{1u}(\pm 1)$. Hence, we introduce a factor g which expresses this anisotropic coupling:

$$\begin{aligned} &\langle {}^3T_{2u} M_s \kappa | \Delta U^{t_{1u}}_{\rho} | {}^3T_{1g} M_s j \rangle \propto \langle {}^3T_{2u} || \Delta U^{t_{1u}} || {}^3T_{1g} \rangle \text{ for } \rho = 0 \\ \text{and} \quad &\langle {}^3T_{2u} M_s \kappa | \Delta U^{t_{1u}}_{\rho} | {}^3T_{1g} M_s j \rangle \propto g \langle {}^3T_{2u} || \Delta U^{t_{1u}} || {}^3T_{1g} \rangle \text{ for } \rho = \pm 1 \end{aligned} \qquad (31)$$

The result is that all transition moments which involve a $t_{1u}(\pm 1)$ component (Table VI.1) are multiplied by a factor g^2.

To illustrate the effect of the anisotropy we calculate first the absorption coefficients $\varepsilon_{//}$ (E//c) and $\varepsilon_{\perp}$ (E⊥c) for the hypothetical case of a single isolated octahedron NiI_6^{4-} with static dipoles m_o (//c) at the iodine ions. The

dipoles cause a splitting of the t_{1u} vibration into two components a_{2u} $(\omega_{//},q_0)$ and e_u $(\omega_\perp,q_{\pm1})$, respectively. The ratio $\varepsilon_\perp/\varepsilon_{//}$ for coupling with $^3T_{1g}$ and $^3T_{2g}$ can be calculated from the transition moments given in Table VI.1, including the factor g:

$$\varepsilon_\perp/\varepsilon_{//} = (5g^2+1)/(2g^2+4) \quad \text{for coupling with } {}^3T_{1g}$$
$$\varepsilon_\perp/\varepsilon_{//} = (g^2+1)/2g^2 \quad \text{for coupling with } {}^3T_{2g} \qquad (32)$$

In Appendix B we will show that the modulation of the crystal-field potential produces an anisotropic coupling with $g^2 >> 1$. Therefore, the fact that the α-polarized spectrum is more intense than the π-polarized spectrum, schematically shown in *Figure VI.7*, indicates that the coupling of the ^1E_g occurs mainly

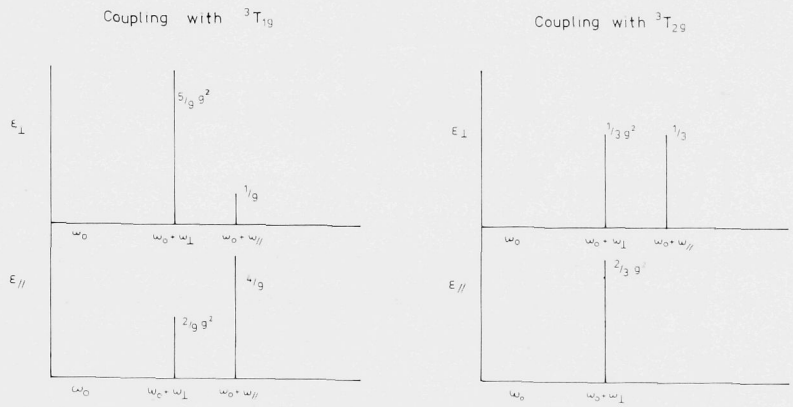

Figure VI.7: Diagram showing the relative contribution of $a_{2u}(\omega_{//})$ and $e_u(\omega_\perp)$ vibrational components to the $^3A_{2g} \rightarrow {}^1E_g$ transition in CdI_2:Ni^{2+} for light polarized parallel ($\varepsilon_{//}$) or perpendicular ($\varepsilon_\perp$) to the trigonal axis.

with the $E_g\,{}^3T_{1g}$ state. The theoretical ratio $\varepsilon_\perp/\varepsilon_{//}$ is 2.5 ($g^2 >> 1$), in very good agreement with the observed ratio 2.4. This is also consistent with the observed positive MCD for the vibronic side band (coupling with $^3T_{1g}$ gives a positive, coupling with $^3T_{2g}$ a negative MCD signal).

The evaluation of the MCD sign and dipole strength of the $a^4T_{1g} \rightarrow b^2T_{1g}$, $^2A_{1g}$ transitions in CdI_2:Co^{2+} is less straightforward, because there are four

possible ungerade intermediate states, which couple the b^4T_{1g} states with a t_{1u} distortion [10].

We are now in a position to evaluate the separate contributions of the modes in the Brillouin Zone (*Figure VI.8*). We have calculated integrated intensities and the separate contributions of the modes as a function of $\underline{k}$ for the high-symmetric directions in the Brillouin Zone. The quantity

$$A^{\beta}_{ki} = \sum_{\rho}\sum_{\rho'} (S^{\rho}_{ki})^* S^{\rho}_{ki} \sum_{a\to b} (B^{\beta\rho}_{ab})^* B^{\beta\rho'}_{ab} \tag{33}$$

describes the contribution of one particular mode i with wave vector k to the absorption coefficient. The contributions to the intensities of the polarized

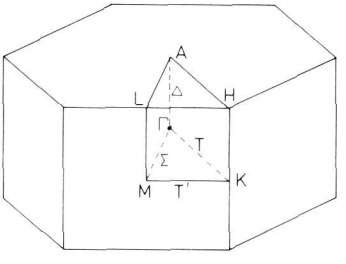

Figure VI.8: Brillouin Zone for the hexagonal Bravais lattice with symmetry lines and points, labelled according to the standard notation. For M $\underline{k} = [0,\frac{1}{2},0]$, *for K* $\underline{k} = [\frac{2}{3},\frac{1}{3},0]$.

spectra, E//c and E⊥c, are $A^{//}_{ki} = A^{o}_{ki}$ and $A^{\perp}_{ki} = \frac{1}{2}(A^{1}_{ki} + A^{-1}_{ki})$. For coupling with $^3T_{1g}$ we find from Table VI.1:

$$\begin{aligned} A^{//}_{ki} &= \frac{1}{54}\left[g^2 \sum_{\rho}|S^{\rho}_{ki}|^2 + (4-g^2)|S^{o}_{ki}|^2\right] \\ A^{\perp}_{ki} &= \frac{1}{54}\left[\frac{5}{2}\,g^2 \sum_{\rho}|S^{\rho}_{ki}|^2 + (1-\frac{5}{2}\,g^2)|S^{o}_{ki}|^2\right] \end{aligned} \tag{34}$$

The total contribution of the acoustic modes (i = 1-3) to the polarized spectra are obtained from the explicit expressions for S^{ρ}_{ki}

$$A^{//}_{k1} + A^{//}_{k2} + A^{//}_{k3} = \frac{2(4+2g^2)}{54\,N\,(M+2m)}\left[(1-\cos ka_1)^2 + (1-\cos ka_2)^2\right] \tag{35}$$

$$A^{\perp}_{k1} + A^{\perp}_{k2} + A^{\perp}_{k3} = \frac{2(1+5g^2)}{54\,N\,(M+2m)} \left[(1-\cos ka_1)^2 + (1-\cos ka_2)^2\right] \tag{36}$$

a_1 and a_2 denote primitive translations.
These equations can be integrated in order to obtain the total absorption due to the acoustic modes in the π- and α-polarized spectra:

$$A^{//}_{ac} \equiv \sum_k (A^{//}_{k1} + A^{//}_{k2} + A^{//}_{k3}) = \frac{6(4+2g^2)}{54\,(M+2m)} \tag{37}$$

$$A^{\perp}_{ac} \equiv \sum_k (A^{\perp}_{k1} + A^{\perp}_{k2} + A^{\perp}_{k3}) = \frac{6(1+5g^2)}{54\,(M+2m)} \tag{38}$$

The results for the infrared modes (i = 4-6) are

$$A^{//}_{k4} + A^{//}_{k5} + A^{//}_{k6} = \frac{2(4+2g^2)}{54\,N\,(\frac{1}{M}+\frac{1}{2m})} \left[\left(\frac{1}{M}+\frac{1}{2m}\right)^2 + \left(\frac{1}{M}+\frac{1}{2m}\cos ka_1\right)^2 + \left(\frac{1}{M}+\frac{1}{2m}\cos ka_2\right)^2\right] \tag{39}$$

$$A^{\perp}_{k4} + A^{\perp}_{k5} + A^{\perp}_{k6} = \frac{2(1+5g^2)}{54\,N\,(\frac{1}{M}+\frac{1}{2m})} \left[\left(\frac{1}{M}+\frac{1}{2m}\right)^2 + \left(\frac{1}{M}+\frac{1}{2m}\cos ka_1\right)^2 + \left(\frac{1}{M}+\frac{1}{2m}\cos ka_2\right)^2\right] \tag{40}$$

The total absorption due to the infrared modes is given by

$$A^{//}_{ir} = \frac{2(4+2g^2)}{54\,(\frac{1}{M}+\frac{1}{2m})} \left(\frac{3}{M^2}+\frac{1}{2m^2}+\frac{1}{mM}\right) \tag{41}$$

$$A^{\perp}_{ir} = \frac{2(1+5g^2)}{54\,(\frac{1}{M}+\frac{1}{2m})} \left(\frac{3}{M^2}+\frac{1}{2m^2}+\frac{1}{mM}\right) \tag{42}$$

The Raman-mode contributions are

$$A^{//}_{k7} + A^{//}_{k8} + A^{//}_{k9} = \frac{4 + 2g^2}{54\,N\,m}(\sin^2 ka_1 + \sin^2 ka_2) \tag{43}$$

$$A^{\perp}_{k7} + A^{\perp}_{k8} + A^{\perp}_{k9} = \frac{1 + 5g^2}{54\,N\,m}(\sin^2 ka_1 + \sin^2 ka_2) \tag{44}$$

The total absorption due to the Raman modes is

$$A^{//}_{Raman} = \frac{(4 + 2g^2)}{54\,m} \tag{45}$$

$$A^{\perp}_{Raman} = \frac{(1 + 5g^2)}{54\,m} \tag{46}$$

The integration of every branch yields the same ratio $A^{//}/A^{\perp} = (4 + 2g^2)/(1 + 5g^2)$, as stated before.

In order to estimate the effect of the mass substitution of Ni^{2+} in CdI_2, PbI_2, and Co^{2+} in CdI_2 we evaluate the relative contributions of the acoustic, Raman and infrared modes. The relative contributions are the same for the α- and π-polarized spectrum, and depend only on the ratio M/2m. *Figure VI.9* shows the result of this calculation. It is clear that the infrared modes are mainly responsible for the intensity in the spectra. However, an increase of the metal-ion mass leads to a strong reduction of the infrared-mode contribution and an enhancement of that of the acoustic modes. The Raman modes appear rather weakly in the spectra.

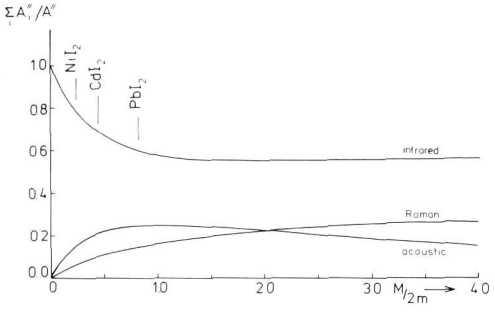

Figure VI.9: Contributions of the acoustic, Raman and infrared mode branches to the intensity of the vibronic side bands of the $^3A_{2g} \rightarrow {}^1E_g$ *transition in* NiI_2, $CdI_2{:}Ni^{2+}$ *and* $PbI_2{:}Ni^{2+}$ *as a function of M/2m.*

Maxima in the absorption are expected from flat regions at symmetry points in the Brillouin Zone, where we can sum over a large number of k values in a narrow frequency range. We have calculated $A^{//}_{ki}$ (i = 1-9) as a function of k for $\Gamma \rightarrow M$ and $\Gamma \rightarrow K$. In *Figure VI.10* the contributions of the acoustic and Raman modes are shown. Transverse or longitudinal modes are indicated

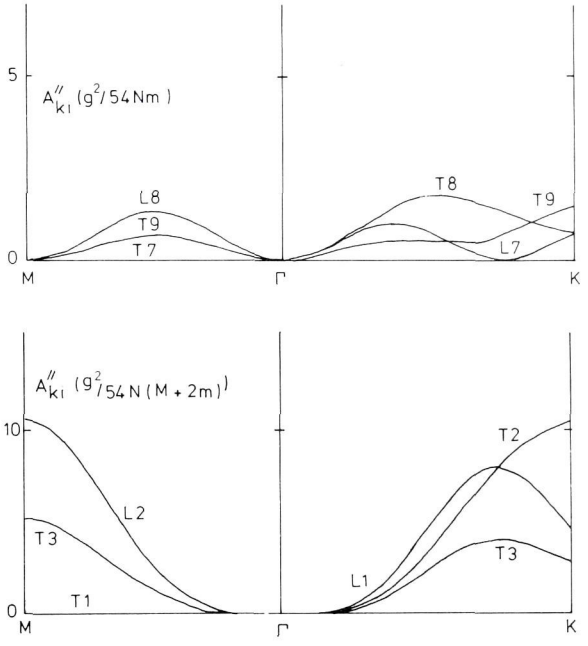

Figure VI.10: Contributions of the acoustic modes i = 1-3 (lower part) and Raman modes i = 7-9 (upper part) as a function of k.

by the T and L, respectively. In *Figure VI.11* the infrared-mode contributions are shown; it is necessary in this case to include explicitely the masses of Ni, Cd, Pb and I.

From $\Gamma \rightarrow M$ the acoustic mode T1(//x) and the Raman mode T7 do not give rise to any absorption. *Figure VI.11* illustrates the small contribution of T6(//z)-type modes for NiI_2, CdI_2 and PbI_2. In the latter compound the absorption is much weaker than in the others. The difference between absorption due to the displacements in the x, y and z direction, respectively, is the smallest in PbI_2.

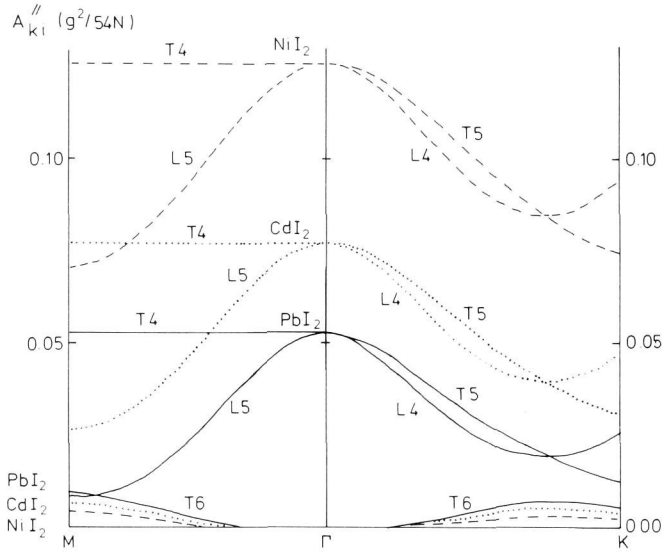

Figure VI.11: Contributions of the infrared modes i = 4-6, as a function of k, calculated for NiI_2 (---), CdI_2 (...) and PbI_2 (——).

VI.4 DISCUSSION

In previous sections we have shown that the maxima of absorption due to one-phonon electric-dipole transitions are expected to correspond to maxima in the phonon density of states of the host crystal. In this section we will assign the observed maxima to phonons corresponding to specific points in the Brillouin Zone.

The phonon frequencies of CdI_2, PbI_2, CoI_2 and NiI_2 are given in Table VI.2. The Raman frequencies of CoI_2 and NiI_2 are not known; the frequencies given in Table VI.2 are those reported for VI_2; these are probably not very different from the frequencies for CoI_2 and NiI_2. The phonon frequencies of CdI_2 at k = 0 and those of NiI_2 and CoI_2 are not very different. Moreover, the higher frequencies of NiI_2 and CoI_2 are presumably reduced, due to smaller force constants and larger induced static dipoles at the iodine ions [17], in CdI_2:Ni^{2+} and CdI_2:Co^{2+}. Therefore, we do not expect that the incorporation of Ni^{2+} and Co^{2+} in CdI_2 leads to local modes. The optical frequencies of NiI_2 and PbI_2 are quite different, but because the effective ionic radius of Pb^{2+} (1.18 Å) is much larger than that of Ni^{2+} (0.700 Å) [22], force con-

TABLE VI.2: Experimental optical frequencies (k = 0) in units of cm^{-1} of CoI_2, NiI_2, CdI_2 and PbI_2. References from which the data were taken, are between brackets.

Optical modes	CoI_2	ref.	NiI_2	ref.	CdI_2	ref.	PbI_2	ref.
E_u^{TO}	152		156		79		52	
		[CH. IV]		[18]		[20]		[20]
E_u^{LO}	175		176		132		108	
A_{2u}^{TO}	185		178		136		96	
		[CH. IV]		[18]		[20]		[20]
A_{2u}^{LO}	191		184		152		121	
E_g	~90		~90		44		74	
		[19]		[19]		[21]		[21]
A_{1g}	~115		~115		112		96	

stants will be strongly reduced in $PbI_2:Ni^{2+}$.

For the assignments of the maxima in the vibronic spectra the compatibility relations are indispensable. These relations show how the space-group representations of the branches in the various directions of the Brillouin Zone are connected. The compatibility relations for the $Cd(OH)_2$ structure, space group D_{3d}^3, calculated with help of the character tables [23], are listed in Table VI.3 for a number a symmetry lines and points.

Because phonon dispersion curves of PbI_2 have been calculated [21,24] and partly measured [25,26], we start to assign the maxima of the spectra of the $^3A_{2g} \rightarrow {}^1E_g$ in $PbI_2:Ni^{2+}$ (*Figure VI.2*). The weak band at 12394 cm^{-1}, which has a MCD sign opposite to that of the vibronic side band, is assigned the zero-phonon transition. According to the overall positive MCD signal the main contributions arise from a e_u-type distortion (Table VI.1); the coupling with a_{2u} would give a negative MCD. The positions of the maxima of the vibronic side band, relative to the frequency of the zero-phonon band, are listed in Table VI.4. The maxima are assigned to space-group representations corresponding mostly to M and K points in the Brillouin Zone. The listed experimental (neutron scattering) and calculated frequencies are obtained from Dorner [25],

TABLE VI.3: Compatibility relations of the $Cd(OH)_2$ structure. The points and lines in the Brillouin Zone are given in standard notation, together with the appropriate factor group and the degeneracy of the star of k. For clearness' sake the point-group representations are given. The mode numbers are those given in Section VI.3.3.

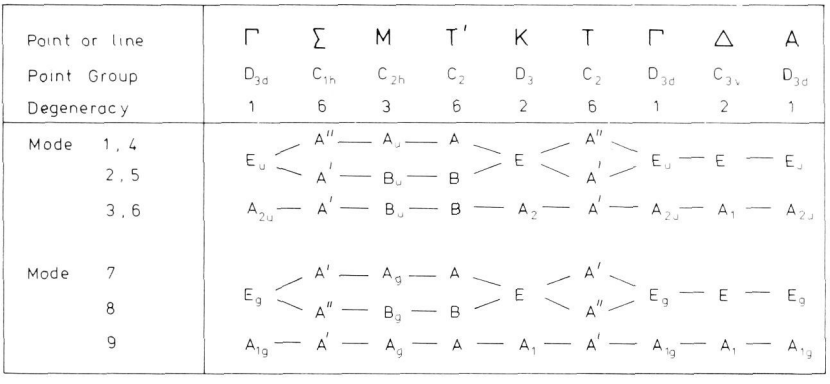

Prévot [26] and Frey [21], respectively. Estimated errors amount to a few wave numbers. The agreement between the positions in the spectrum of PbI_2:Ni^{2+} and the experimental and calculated frequencies of the modes in PbI_2 is very good.

Due to the low frequency of the E_u^{TO} mode (52 cm^{-1}) and the strongly reduced nearest-neighbour force constants, the low-energy part of the spectrum is enhanced in intensity. As the main contributions arise from the E_u modes (positive MCD signal), the peak at 22 cm^{-1} should be assigned to L_4, because $K_2(A_{2u}^{TA})$ would produce a negative MCD. The mode frequency at L_4 is not known but can be estimated from the acoustic mode at M and A [21], which have frequencies of 29 and 14 cm^{-1}, respectively.

The bands at about 69 cm^{-1} and 80 cm^{-1} are weak; although the contribution of the Raman modes at point M was calculated to be zero, some intensity may be obtained on the Σ line, where mixing of ungerade and gerade modes is allowed. Surprisingly large is the peak intensity at 91 cm^{-1}. We do not understand the large intensity of this mode; the frequency corresponds to an A_{1g} mode at the Γ point.

The vibronic bands of the $^3A_{2g} \rightarrow {}^1E_g$ transition in CdI_2:Ni^{2+} are shown in *Figure VI.1* and Table VI.5. The weak band at 12441 cm^{-1} was assigned to

TABLE VI.4: Assignments of the maxima of the $^3A_{2g} \rightarrow {}^1E_g$ transition of PbI_2: Ni^{2+} to vibrational modes listed according to their space-group representation. The corresponding point-group representations of D_{3d} are also given. A comparison between the relative positions in the vibronic spectrum with respect to the zero-phonon band (ν_o = 12394 cm^{-1}) and experimental [25,26] and calculated [21] phonon frequencies of PbI_2 is made.

Relative position (cm^{-1})	Space-group representation	Exp. (*) or calc. frequency (cm^{-1})	Point group D_{3d} representation
22	L_4	-	$E_u + A_{2u}$
	K_2	22*	$A_{2u} + A_{2g}$
28	M_4	29*	$E_u + A_{2u}$
44	K_3	45*	$E_u + E_g$
49	M_4	50*	$E_u + A_{2u}$
54	K_2	54	$A_{2u} + A_{2g}$
	M_2	56*	$E_u + A_{1u}$
69	K_3	66	$E_u + E_g$
	A_3	68	E_g
	M_1	71*	$E_g + A_{1g}$
	M_3	71*	$E_g + A_{2g}$
80	K_1	78	$A_{1g} + A_{1u}$
	M_1	83	$A_{1g} + E_g$
91	A_1	91	A_{1g}
110	$E_u^{LO}\ \Sigma_1$	104	E_u
	$E_u^{LO}\ T_1$		E_u
117	$A_{2u}^{LO}\ \Delta_1$	118	A_{2u}
	M_4	119	$E_u + A_{2u}$

TABLE VI.5: Assignments of the maxima in the vibronic spectra of $CdI_2:Co^{2+}$ and

$CdI_2:Co^{2+}$		
Relative position (cm^{-1}) $a^4T_{1g}(E'_g) \longrightarrow {}^2A_{1g}(E'_g)$ $\nu_o = 15669\ cm^{-1}$	Relative position (cm^{-1}) $a^4T_{1g}(E'_g) \longrightarrow b^2T_{1g}(U'_g)$ $\nu_o = 15280\ cm^{-1}$	Relative position (cm^{-1}) $a^4T_{1g}(E'_g) \longrightarrow b^2T_{1g}(E'_g)$ $\nu_o = 15376\ cm^{-1}$
21	-	-
40	35	-
47	-	-
-	60	64
69	68	72
73 81	78	79
100	87	89
100	107	108
115 120	112	112
130	129	129
141	138	138

$CdI_2:Ni^{2+}$. Positions are given relative to the zero-phonon origin ν_o.

$CdI_2:Ni^{2+}$		
Relative position (cm^{-1}) $^3A_{2g}(T_{2g}) \longrightarrow {}^1E_g(E_g)$ $\nu_o = 12441\ cm^{-1}$	Space-group representation	Point-group D_{3d} representation
-	L_4 K_2	$E_u + A_{2u}$ $A_{2u} + A_{2g}$
37	K_3 M_3	$E_u + E_g$ $E_g + A_{2g}$
-	local mode?	t_{2u} (?)
59	M_4 (M_1)	$E_u + A_{2u}$ $E_g + A_{1g}$
67	K_3	$E_u + E_g$
76	M_2 $E_u^{TO}\ \Delta_3$ K_3	$E_u + A_{1u}$ E_u $E_u + E_g$
99	M_2 K_1 (M_1)	$E_u + A_{1u}$ $A_{1u} + A_{1g}$ $A_{1g} + E_g$
103	M_4 K_2	$A_{2u} + E_u$ $A_{2u} + A_{2g}$
117	K_3	$E_u + E_g$
131	M_4 $E_u^{LO}\ \Sigma_1$ $E_u^{LO}\ T_1$	$E_u + A_{2u}$ E_u E_u

the zero-phonon transition. The vibronic frequencies obtained from the CdI_2:Ni^{2+} spectrum are compared in Table VI.5 with the frequencies obtained from the CdI_2:Co^{2+} $a^4T_{1g}E'_g \rightarrow b^2T_{1g}U'_g$, E'_g and $a^4T_{1g}E'_g \rightarrow {}^2A_{1g}E'_g$ transitions (*Figures VI.3* and *VI.4*, respectively). The absorptions at 15280, 15376 and 15669 cm^{-1} were assigned to the zero-phonon transitions. The first two transitions are intraconfigurational transitions within the strong-field configuration $t_{2g}e_g^2$; the third transition is an interconfigurational transition between $t_{2g}e_g^2$ and $t_{2g}^2e_g$.

The phonon dispersion curves of CdI_2 are not known. Calculations are not available, and the experimental determination with inelastic neutron scattering is hampered by the large neutron absorption of Cd. We have used the observed maxima of the vibronic spectra to estimate the phonon dispersion curves of CdI_2. For this purpose we have used the frequencies of the zone-center modes (Table VI.2), the compatibility relations (Table VI.3) and also the comparison with PbI_2. An important difference between the phonon branches of CdI_2 and PbI_2 is caused by the reversal of the E_u^{TO} and E_g frequencies.

From these considerations the vibrational branches of CdI_2 have been deduced, as shown in *Figure VI.12*. The assignment of the observed maxima is given

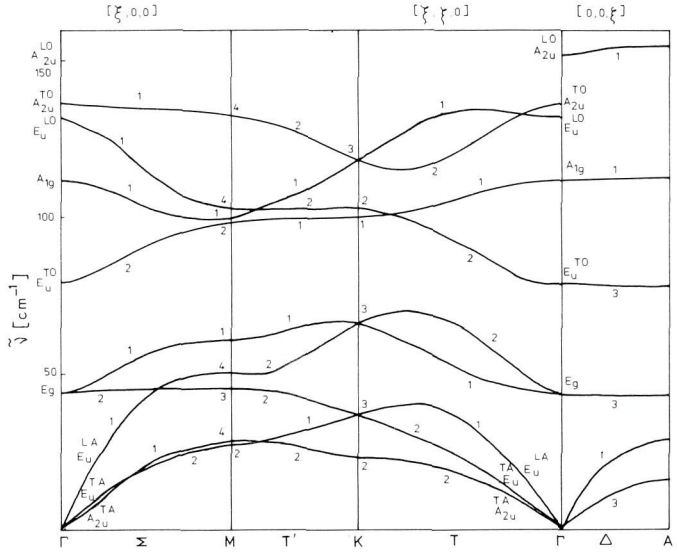

Figure VI.12: Dispersion of the acoustic and optic branches of CdI_2 as deduced from the vibronic fine structure of the ${}^3A_{2g} \rightarrow {}^1E_g$ transition. The numbers indicate the space-group representations.

in Table VI.5. Weak absorptions due to acoustic and Raman modes are observed only in a few cases. Those modes at the M point which have been calculated zero are put between brackets (fifth column of Table VI.5). A possible peak at 99 cm^{-1} in the spectrum of the $a^4T_{1g}E'_g \rightarrow b^2T_{1g}U'_g$ transition is overlapped by the zero-phonon band of the $b^2T_{1g}E'_g$ transition.

The correspondence between the four spectra is remarkable, and it shows indeed that the host lattice CdI_2 is responsible for the observed fine structure. The spectrum of the $a^4T_{1g} \rightarrow {}^2A_{1g}$ is broadened and presumably also shows contributions of two-phonon processes (*Figure VI.4*).

As shown by the calculation in the previous section a reduction of the intensities from α to π polarization of about 60% is expected for the ${}^3A_{2g} \rightarrow {}^1E_g$ transition, if the coupling of ${}^1E_g$ is mainly with the ${}^3T_{1g}$ state (*Figure VI.1*) and the vibronic coupling is due to the e_u component of the t_{1u} distortions. A positive MCD is calculated in this case as is observed for the entire vibronic spectrum of the ${}^3A_{2g} \rightarrow {}^1E_g$ transition. An exception is band 7 (103 cm^{-1}) which does not reduce in intensity from α to π polarization. Band 7 is assigned to a mainly A_{2u}-type vibration. For a pure A_{2u}-type contribution, an enhancement of the intensity by a factor 4 from α to π polarization is expected. We remark that the selection rules are not strictly valid; at arbitrary points in the Brillouin Zone, mixing of all vibrational modes occurs, and this will lead to (small) contributions of other modes to the vibronic side band.

The ${}^4T_{1g} \rightarrow {}^2A_{1g}$ transition shows a very narrow σ-polarized band at 47 cm^{-1} with respect to ν_o = 15669 cm^{-1}. The origin of this peak is not clear; it could be related to a local mode.

VI.5 REFERENCES

1. R.W.G. Wyckhoff, *Crystal Structures*, Vol. I, Interscience, New York (1963).
2. W.E. Bron and M. Wagner, *Phys. Rev.* A139, 233 (1965).
3. R.A. Satten, *J. Chem. Phys.* 40, 1200 (1964).
4. A.S. Barker and A.J. Sievers, *Rev. Mod. Phys.* 47, Suppl. No. 2, S1 (1975).
5. N.B. Manson and K.Y. Wong, *J. Phys.* C8, L73 (1975).
6. N.B. Manson and K.Y. Wong, *J. Phys.* C9, 611 (1976).
7. M.J.L. Sangster and C.W. McCombie, *J. Phys.* C3, 1498 (1970).
8. S.R. Kuindersma and P.R. Boudewijn, *Solid State Commun.* 27, 1181 (1978).
9. P.R. Boudewijn, Thesis, Groningen (1980).
10. P.R. Boudewijn, A. Meetsma and C. Haas, to be published.
11. P.N. Schatz and A.J. McCaffery, *Quart. Rev. Chem. Soc.* 23, 552 (1969).

12. M. Born and J.R. Oppenheimer, *Ann. Physik* 84, 457 (1927).
13. M.J. Harding, S.F. Mason, D.J. Robbins and A.J. Thomson, *J. Chem. Soc. (A)*, 3047 (1971).
14. D.B. Bird, G.A. Osborne and P.J. Stephens, *Phys. Rev.* B5, 1800 (1972).
15. J.S. Griffith, *The Irreducible Tensor Method for Molecular Symmetry Groups*, Prentice-Hall, Englewood Cliffs, N.J. (1962).
16. S.R. Kuindersma, P.R. Boudewijn and C. Haas, to be published.
17. H.J.L. van der Valk and C. Haas, *Phys. Status Solidi (b)* 80, 321 (1977).
18. S.R. Kuindersma, W.R. Müller and M. Rautenberg, *International Conference Lattice Dynamics*, Ed. M. Balkanski, p. 613, Paris (1977).
19. G. Güntherodt, W. Bauhofer and G. Benedek, *Phys. Rev. Lett.* 43, 1427 (1979).
20. G. Lucovsky and R.M. White, *Il Nuovo Cimento* 38B, 290 (1977).
21. A. Frey and R. Zeyher, *Solid State Commun.* 28, 435 (1979).
22. R.D. Shannon and C.T. Prewitt, *Acta Cryst.* B25, 925 (1969).
23. C. Bradley and A.P. Cracknell, *The Mathematical Theory of Symmetry in Solids*, Clarendon Press, Oxford (1972).
24. A. Frey, Thesis, Stuttgart (1977).
25. B. Dorner, R.E. Ghosh and G. Harbeke, *Phys. Status Solidi (b)* 73, 655 (1976).
26. B. Prêvot, J. Biellmann, B. Dorner and A. Frey, *Solid State Commun.* 35, 31 (1980).

VI.6 APPENDIX A: V Coefficients for the complex trigonal component system

V Coefficients are defined by Griffith [1] and in his book tables of V are presented for different component systems. However, some of his tables of V coefficients for the complex trigonal component system are in error and we will present here the corrected tables. Components are ordered as 1, 0, -1.

$$V\begin{pmatrix} T_1 & T_1 & T_1 \\ \alpha & \beta & \gamma \end{pmatrix} = V\begin{pmatrix} T_1 & T_2 & T_2 \\ \alpha & \beta & \gamma \end{pmatrix} = (1/\sqrt{6})\varepsilon_{\alpha\beta\gamma}{}^{*}$$

A_1 T_1 T_1 or A_1 T_2 T_2 or A_2 T_1 T_2	V
1 1 -1	$1/\sqrt{3}$
1 0 0	$-1/\sqrt{3}$
1 -1 1	$1/\sqrt{3}$

E E	V: E: A_1	A_2	1	-1
1 1	0	0	$-i/\sqrt{2}$	0
1 -1	$1/\sqrt{2}$	$-i/\sqrt{2}$	0	0
-1 1	$1/\sqrt{2}$	$i/\sqrt{2}$	0	0
-1 -1	0	0	0	$i/\sqrt{2}$

E T_1 T_1 or E T_2 T_2	V
1 1 1	$-i/\sqrt{6}$
-1 -1 -1	$i/\sqrt{6}$
-1 1 0	$-i/\sqrt{6}$
-1 0 1	
1 -1 0	
1 0 -1	

T_1 T_1 T_2 or T_2 T_2 T_2	V
0 0 0	$i\sqrt{2}/3$
1 1 1	$-i\sqrt{2}/3$
-1 -1 -1	$i\sqrt{2}/3$
0 1 -1	$i/3\sqrt{2}$
0 -1 1	
1 0 -1	
-1 0 1	
1 -1 0	
-1 1 0	

E T_1 T_2	V
-1 -1 -1	$-1/\sqrt{6}$*
1 1 1	$-1/\sqrt{6}$*
-1 0 1	$1/\sqrt{6}$
1 0 -1	$-1/\sqrt{6}$
-1 1 0	$1/\sqrt{6}$
1 -1 0	$-1/\sqrt{6}$

* Different from Table C2.4 of reference [1].

Reference

1. J.S. Griffith, *The Irreducible Tensor Method for Molecular Symmetry Groups*, Prentice-Hall, Englewood Cliffs, N.J. (1962).

VI.7 APPENDIX B: Modulation of the cubic crystal-field potential by a t_{1u} vibration

In order to calculate the matrix elements of the vibronic coupling operator $< {}^{2S+1}\Gamma_u|U|{}^{2S+1}\Gamma'_g >$, the change of the crystal field due to t_{1u} vibrations has to be evaluated. For this we will use the polarizable-ion model in which the metal ion has an effective (Szigeti) charge +2Z and the anions a charge -Z; the electronic polarizability of the anions is α.

The matrix elements contain wave functions which are defined with respect to the position R_M of the central metal atom:

$$< {}^{2S+1}\Gamma_u(r-R_M)|U(r)|{}^{2S+1}\Gamma'_g(r-R_M) \qquad (1)$$

We define a coordinate r' which gives the position of the electron with respect to the cation nucleus: $\underline{r'} = \underline{r} - \underline{R}_M$. We consider contributions to U(r) from the charges Z_i and the induced dipoles m_i on ligand ions i. Only nearest neighbours are considered (i = 1-6).

$$U(r) = \sum_i \frac{Z_i e}{|r - R_i|} + \sum_i \underline{m}_i \frac{\underline{r} - \underline{R}_i}{|r - R_i|^3} \qquad (2)$$

We evaluate the change ΔU caused by small displacements $u_{i\alpha}$ and $u_{M\alpha}$ of the nuclei from the equilibrium positions R^0_i and R^0_M:

$$\begin{aligned} R_{i\alpha} &= R^0_{i\alpha} + u_{i\alpha} \\ R_{M\alpha} &= R^0_{M\alpha} + u_{M\alpha} \end{aligned} \qquad (3)$$

with α = x,y,z. We choose the equilibrium position of the central metal ion as the origin which means that $R^0_M = 0$ and $R_{M\alpha} = u_{M\alpha}$. Equation (2) is now expanded and the terms linear in the displacements are retained. There is an extra term in ΔU which arises from the change of the induced dipole moments by the vibration. The total induced moment is $\underline{m}_i = \alpha \underline{E}_i$ where $\underline{E}_i$ is the total electric field at ligand i, position $\underline{R}_i$. The field $\underline{E}_i$ is also expanded in small displacements of the nuclei, which results in an extra contribution to ΔU. From this term and the expansion of equation (2) we obtain for a t_{1u} vibration:

$$\Delta U^{t_{1u}}(r' + R_M) = \sum_i \sum_\alpha G_{i\alpha}\,(u_{i\alpha} - u_{M\alpha}) \tag{4}$$

where we have substituted $Z_i = -Z$ and $Z_M = +2Z$ and $|R_i^0| = R_0$. Ignoring terms with $(u_{i\alpha} - u_{j\alpha})$ which do not contribute to a t_{1u} vibration $G_{i\alpha}$ is given by:

$$G_{i\alpha} = -\frac{Ze(r'_\alpha - R^0_{i\alpha})}{|r' - R_i^0|} - \frac{m_{i\alpha}}{|r' - R_i^0|^3} + \frac{3m_{i\beta}(r'_\beta - R^0_{i\beta})(r'_\alpha - R^0_{i\alpha})}{|r' - R_i^0|^5} +$$

$$- \frac{2Ze\alpha(r'_\alpha - R^0_{i\alpha})}{R_0^3|r' - R_i^0|^3} + 6Ze\alpha \sum_\beta \frac{R^0_{i\alpha}R^0_{i\beta}(r'_\beta - R^0_{i\beta})}{R_0^5|r' - R_i^0|^3} \tag{5}$$

The function $G_{i\alpha}(r')$ is now expanded for small values of r' and only terms linear in r' are retained. The $G_{i\alpha}$ terms may then be calculated by substituting values of the coordinates $R^0_{i\alpha}$ and the dipole moments $m_{i\alpha}$. The displacements $u_{i\alpha}$ and $u_{M\alpha}$ are transformed to the t_{1u} normal coordinates q_0 and $q_{\pm 1}$. The resulting expression for the modulation of the crystal field due to a t_{1u} vibration is:

$$\Delta U^{t_{1u}} = C\, r'_z\, q_0 + g\, C\, (\omega r'_- q_1 + \omega^2 r'_+ q_{-1}) \tag{6}$$

with $$C = \frac{2\sqrt{6}Ze}{3R_0^3}\left(1 - \frac{4\alpha}{R_0^3}\right) \quad ; \quad \omega = \exp(2\pi i/3)$$

and $$g = 1 + \frac{3\sqrt{3}m_0}{2ZeR_0}\left(\frac{1}{1-(4\alpha/R_0^3)}\right)$$

An anisotropic coupling results, if g deviates from one. This anisotropy is due to the static dipole moments m_o at the iodine ions and is independent of the magnitude of the charge Z (m_o is proportional to Z).

Using the values of NiI_2 [1], CdI_2 and PbI_2 [2] for the parameters α, g is calculated as -8.35 for NiI_2, +6.49 for CdI_2 and +7.59 for PbI_2. This shows that the coupling is very anisotropic in these cases, with stronger coupling to the $e_u(t_{1u} \pm 1)$ modes than to the $a_{2u}(t_{1u}0)$ modes.

References

1. S.R. Kuindersma, W.R. Müller and M. Rautenberg, *International Conference Lattice Dynamics*, Ed. M. Balkanski, p. 613, Paris (1977).
2. H.J.L. van der Valk and C. Haas, *Phys. Status Solidi (b)* 80, 321 (1977).